Journal of Materials Chemistry A

ROYAL SOCIETY OF CHEMISTRY

PAPER

View Article Online
View Journal

Cite this: DOI: 10.1039/d5ta07754k

Development and performances analysis of eco-friendly pullulan/ polyvinyl alcohol composites based all-solid-state supercapacitors

Elyes Bel Hadj Jrad,[ac] Francesca Soavi *[b] and Chérif Dridi*[a]

Next-generation electronic devices, including embedded microsystems and wearable technologies, require the development of safe, and low-cost energy storage systems to meet the 21st-century society demands. In this context, several ecological binders have been developed and amended in order to achieve high-performance carbon-based supercapacitors. This work demonstrates a solid state-based supercapacitor using Pullulan (Pu)/Polyvinyl Alcohol (PVA) composite as an eco-friendly binder for the first time, for carbon-based electrodes development. Furthermore, PVA/KOH/Glycerol (GCy) blends are used as conductive electrolytes towards safe and light weight devices manufacturing. The electrodes are fabricated through simple and low-cost hand-painting (paint brush) on Nickel foam substrates. The device shows an interesting areal capacitance of 176 mF cm^{-2} at 10 mV s^{-1}, energy and power densities of 25 μWh cm^{-2} and 3.2 mW cm^{-2} respectively, at 0.5 A g^{-1}. More importantly, the device demonstrates robust mechanical strength with excellent reversibility across various bending angles (0°, 90°, 180°), with a capacitance retention of 90% after 10 000 charging/discharging cycles while maintaining an important coulombic efficiency (>95%). The outcomes of this work are quite promising compared to many reported studies, opening wide potential application in the field of handheld electronics.

Received 22nd September 2025
Accepted 10th February 2026

DOI: 10.1039/d5ta07754k

rsc.li/materials-a

1 Introduction

The supercapacitor (SC) market is estimated to reach 912 million USD in 2027, instead of 472 USD millions in 2022, within a Compound Annual Growth Rate (CAGR) of 14.1% in all over the world.[1] In fact, electrical double layered capacitors (EDLCs) present the largest market share segment for their high power and long life-cycle. The long-standing conventional orientation for the prosperity and improvement purposes of commercial supercapacitors relies on nanocomposite materials and innovative electrolytes integration towards boosting their energetic performances. However, in light of numerous studies addressing environmental challenges and evolving patterns in global electricity consumption, as reported by the International Energy Agency (IEA),[2] it is necessary to emphasize the integration of ecological and green materials towards low cost and environmentally friendly energy harvesting/storage devices.[3] Furthermore, today's innovative scientific research is interested particularly, in lightweight supercapacitors to answer the needs of the next generation technology.

Supercapacitors are classified into EDLCs, pseudocapacitors, and hybrid supercapacitors based on their charge storage mechanisms, while solid-state supercapacitors (SSCs) follow the same classification but utilize solid or gel polymer electrolytes instead of liquid ones, offering improved safety, flexibility, and stability. In fact, Solid-State Supercapacitors (SSCs) are advanced energy storage devices that operate based on two primary charge storage mechanisms: EDLC, which relies on the physical adsorption of ions at the electrode/electrolyte interface, and pseudocapacitance, which involves fast, reversible redox reactions on the electrode surface. SSCs typically incorporate dry solid polymer electrolytes (SPEs), gel polymer electrolytes (GPEs), or inorganic electrolyte, which provide moderate ionic conductivity and wide operating potential window, while eliminating leakage risks associated with liquid electrolytes.[4] This design enables the development of lightweight and thin energy storage devices suitable for wearable electronics and portable devices. The performance of SSCs is heavily influenced by the electrode materials, often nanostructured carbons, metal oxides, or conductive polymers, as well as the ionic mobility within the solid electrolyte matrix. Despite their advantages in safety, mechanical robustness, and design versatility, SSCs face challenges such as relatively lower specific capacities and energy densities compared to their liquid-based counterparts.[5] Therefore, several studies focused on the development of

[a]NANOMISENE Laboratory LR16CRMN01, Center for Research in Microelectronics and Nanotechnology of Sousse, Sahloul Sousse 4054, Tunisia. E-mail: Cherif.Dridi@crmn.rnrt.tn

[b]Department of Chemistry "Giacomo Ciamician", Laboratory of Electrochemistry of Material for Energetics, Alma Mater Studiorum, Universita' di Bologna, Italy. E-mail: Francesca.soavi@unibo.it

[c]Higher School of Science and Technology of Hammam Sousse, Hammam Sousse 4011, Tunisia

supercapacitor's electrodes using metals and metal oxides for high-performance energy storage devices manufacturing. These materials are known for their excellent electrical conductivity, high specific capacitance, and robust electrochemical stability.[6–8] Despite their advantages, metals and metal oxides face challenges such as poor cycling stability due to structural degradation during charge–discharge cycles, limited rate capability caused by sluggish ion diffusion in bulk materials, and potential agglomeration or volume changes that can compromise electrode integrity and performance over time.[9] In this context, Activated Carbon (AC) was widely used for supercapacitors electrodes development. The high porosity, different pore size distribution, high specific surface and more importantly the low-price,[10] made AC a suitable and safe material that can be recognized in several fields including, water remediation, gases filtering, health-care area, medical applications, energy storage devices and many others.[11–13]

The fabrication of supercapacitor electrodes heavily relies on conventional binders like Polyvinylidene Fluoride (PVDF) and Polytetrafluoroethylene (PTFE) which present significant challenges, including the requirement of toxic organic solvents, such as *N*-methyl-2-pyrrolidone (NMP) and Dimethyl Sulfoxide (DMSO) that raises environmental and safety concerns.[14] Therefore, several ecological binders such as CarboxyMethyl Cellulose (CMC), Styrene Butadiene Rubber (SBR), Gelatine, Chitosan and Casein were investigated for the preparation of carbon-based electrodes.[15] Pullulan (Pu) and Polyvinyl Alcohol (PVA) share a wide number of physicochemical properties such as the biocompatibility, biodegradability and non-toxicity, which made them quite promising materials for the energy storage field development. In addition, both Pu and PVA, even mixed with glycerol (GCy) plasticizer, demonstrated high thermal stability above 200 °C.[16–18] Pu has been used as a green binder for the first time for a highly voltage (3.2 V) Pu-Ionic Liquid-EDLC supercapacitors in ref. 17–19. A. Brilloni *et al.* compared the use of Pu as a water-processable binder to PVDF for Lithium metal batteries.[16,20] Additionally, poly(vinyl alcohol) (PVA) composites have been already widely used as eco-friendly binders for electrodes development, in particular for solid state supercapacitors manufacturing.[16,21] However, in contrast to PVA, Pu based films exhibit some important limitations such as brittleness and poor mechanical strength.[22] More importantly, the poor water resistance of Pu makes its use irrelevant for supercapacitors development when aqueous and/or water-based electrolytes are employed. Therefore, the incorporation of Pu based carbon electrodes on aluminium foils in a bendable and lightweight solid state supercapacitor configuration was recently reported by our team,[23] in order to prevent films degradation issues in water-based mediums. The device was assembled using PVA/KOH-GCy solid electrolyte featuring an ionic conductivity of 3.6 mS cm^{-1} at room temperature. The supercapacitor showed a areal capacitance of 155 mF cm^{-2} at 5 mV s^{-1}, with an excellent stability (>91% after 9000 cycles) at an operating potential of 1.4 V. Notably, Pu based device demonstrated important energetic performances compared to other studies reported in literature, unveiling the significant potential of Pu in supercapacitor manufacturing and energy storage prosperity.

Nevertheless, and as far as we know, Pu/PVA composites have never been published as potential binders for supercapacitors and/or batteries applications. First of all, the incorporation of PVA into pullulan significantly enhanced the thermal stability of the membranes, indicating that the improved thermal behaviour of the Pu/PVA blend system can be attributed to the presence of PVA, in agreement with the findings reported by M. R. Karim *et al.*[24] The composite experience primary decomposition between 250–400 °C.[24] This enhanced thermal stability is beneficial for supercapacitor applications, where materials experience elevated temperatures during operation and cycling.

Besides, many works have been reported towards the improvement of thermoplastic and water resistance properties of such blends towards more sustainable, robust and stable films. For instance, Iuliana S. *et al.* reported the excellent stability of Pu/PVA hydrogels blends against dissolution in water for Adipose Tissue Engineering.[25] Naozumi T. *et al.* studied the morphological and mechanical properties Pu-PVA blends doped with Glyoxal.[26] Pu/PVA/Montmorillonite[27] and PVA/Pu/Ag[28] nanofibers were also elaborated through electrospinning method for several prospective uses. More importantly, researchers are increasingly focusing on developing novel techniques for supercapacitors electrodes manufacturing using simple, low-cost manufacturing approaches that do not require complex instruments or stringent conditions, such as screen printing and electrodeposition techniques. This shift aims to enhance the scalability and commercial viability of supercapacitors while reducing production costs.

Therefore, this work demonstrates the Pu blending strategy with PVA polymers towards biocompatible and environmentally friendly binders for all carbon-based electrodes development for the first time as far as we know. Indeed, this work focuses on three main strategic aspects: ecological sustainability, economic efficiency, and electrochemical performance. From an ecological perspective, the use of Pu, PVA, and their blends as binders avoid conventional perfluorinated binders such as PTFE and PVDF, which require toxic organic solvents like NMP. Replacing these materials with water-soluble biopolymers represents a more sustainable and environmentally friendly approach. Economically, Pu and PVA offer a significant cost advantage over conventional binders and solvents. For example, considering costs claimed by today's chemical providers at a lab-scale, in a conventional process, the combined cost of 1 g of PTFE (1.75 €) and 1 mL of NMP (0.68 €) reaches approximately 2.43 €, excluding carbon and substrate costs. In contrast, 1 g of Pu (0.21 €) or PVA (0.30 €) can be dissolved directly in distilled water, resulting in a substantially lower overall cost. In addition, the electrodes are fabricated using a simple solution-casting method with a conventional hand brush, avoiding complex and energy-intensive techniques such as doctor-blade coating. Finally, blending Pu with PVA serves two key purposes: (i) enhancing the mechanical stability of Pu, which is inherently brittle compared to PVA, and (ii) mitigating Pu degradation in aqueous environments and water-based

electrolytes, thereby improving electrode durability and performance. This strategy further opens new opportunities for the development of advanced Pu-based carbon electrodes with potential applications in next-generation, sustainable energy storage devices.

The carbon films were successfully coated on Nickel foam substrates. Solid state supercapacitors devices were developed using PVA/KOH blends plasticized with Glycerol (GCy) as ionic conductive mediums. What's more, the built-in strength, the high porous structure and the excellent electrical conductivity of Nickel foams made it possible to achieve safe and light weight devices opening a great potential application in several fields including smart textile and wearable devices. This work aligns with the United Nations Sustainable Development Goals, particularly SDG 7 (Affordable and Clean Energy) and SDG 11 (Sustainable Cities and Communities), by promoting environmentally friendly, low-cost electrode materials and fabrication processes for sustainable energy storage applications.

2 Experimental section

PVA (M_w = 89.000–98.000 g mol^{-1}, 99 + % hydrolyzed) and GCy (M_w = 92.09 g mol^{-1}, Purity >99%) were both procured from Sigma-Aldrich. Pu powders were purchased from the Tokyo Chemicals Industry (TCI). Commercial AC (YP80F-05120 KURARAY, 2400 m^2 g^{-1})[29] and Carbon black (Super C45, Imerys, Paris, France) were used for the supercapacitor's electrodes fabrication. Nickel foams (diameter 0.9 cm) were obtained from Alantum industries in Germany.

2.1 Carbon-based electrodes preparation

Carbon based films on nickel foams substrates were prepared as follows. Pu powder was mixed with GCy at a mass ratio of 1 : 1, then dissolved in 1 mL of MilliQ water. The mixture was maintained under constant stirring at room temperature until a transparent and homogeneous solution was obtained. Subsequently, a mixture of Activated Carbon (YP80F) and carbon black (C45) (as conducting additive) was introduced. The continuous agitation results in a carbon ink like solution. Similarly, Pu/PVA-Carbon based electrodes were prepared by dissolving 0.5 g of PVA in a small amount of distilled water (5 wt%). After two hours of constant stirring (300 rpm) at 95 °C, GCy was added, and the mixture was stirred to form a composition of 80 : 20% of PVA to GCy. Thereafter, 42 mg of Pu and 42 mg of PVA/GCy were mixed within 2 g of MilliQ water. AC and CB were slowly added to form a ratio of 70 : 30% (Carbon:-Binder). The beaker was covered to limit the solvent evaporation and the mixture was kept under stirring for almost 24 hours until a carbon-ink like solution was obtained.

Afterwards, both solutions were hand painted gently on the nickel foams (1 cm × 0.5 cm) using a cleaned paint brush. Pu-C and Pu/PVA-C based electrodes were then dried at room temperatures and subsequently kept in an oven at 60 °C and 80 °C overnight respectively. The composite electrode loading (excluding the Nickel foam mass) was in the range of 2 to 2.3 mg on a surface of 0.5 cm^2 and a thickness of 13 μm to 21.5 μm for both samples. As a result, the capacities of the two electrodes are expected to be well matched, and the N/P ratio is therefore close to unity (N/P ≈ 1). To simplify, both supercapacitors will be denoted as Pu-D and Pu/PVA-D referring to Pu-C and Pu/PVA-C based electrodes.

2.2 PVA-GCy/KOH blends preparation

The electrolyte blend was prepared as follows. Briefly, 1 g of PVA powder was vigorously stirred in 20 mL of distilled water (95 °C, 2 hours). Once the solution was cooled at room temperature, GCy was introduced to form a 80 : 20% of PVA : GCy mixture. A solution of 3 M of KOH was prepared separately then added slowly (dropwise) to the mixture under stirring to produce a 60 : 40% PVA-GCy : KOH solution. Continuous agitation lasted for almost 3 hours before putting the prepared viscous solution in a Petri dish to dry at room temperature overnight. The PVA-GCy/KOH film is denoted as PGK for the rest of the study.

2.3 Characterization setup

Scanning Electron Microscopy (SEM) was performed to provide detailed morphological information on the elaborated carbon-based films using an Apero 2S FEI (ThermoFisher Scientific) instrument at an acceleration voltage of 15 kV. FTIR measurements were performed to identify and analyze the chemical composition and functional groups of Nickel foam, Pu-Carbon and Pu@PVA-Carbon samples on Nickel foams substrates. All FTIR spectrums were recorded using a "PerkinElmer's Spectrum Two™ IR"spectrometer at room temperature by applying an infrared radiation at wavelength range from 4000 to 500 cm^{-1}.

Electrochemical measurements including Electrochemical Impedance Spectroscopy (EIS), Cyclic Voltammetry (CV) and Galvanostatic Cycling with Potential Limitation (GCPL) were performed for the 2- and 3 electrodes setups. All electrochemical analyses were conducted at ambient temperature (22 ± 2 °C) using a BioLogic VSP multichannel potentiostat/galvanostat/FRA workstation. A 3-electrodes system was made using a T Swagelok-type configuration (BOLA Cell made from Teflon, BOLA GmbH, Grünsfeld -Germany, electrode area 0.63 cm^2) with Pu-Carbon and/or Pu/PVA-Carbon as working electrodes, Teflon-Carbon self-standing films as reference electrodes. Stainless-steel pistons were used as current collectors for both sides. Platinum wire was integrated gently as counter electrode for the complete circuit building. Simultaneously, symmetric solid-state supercapacitors were manufactured within a sandwich structure in which the PGK film was integrated between both carbon-based electrodes (Pu-C or Pu/PVA-C). For flexibility tests and to make easily operated devices, the supercapacitors were encapsulated using Kapton® polyimide flexible film tape to ensure excellent mechanical integrity and physical stability. The KPIs of Pu-C and Pu/PVA-C symmetrical devices, abbreviated as Pu-D and Pu/PVA-D, were evaluated for comparison purposes. Carbon electrodes preparations, electrolyte synthesis and electrochemical measurement setups are illustrated in Fig. 1 below.

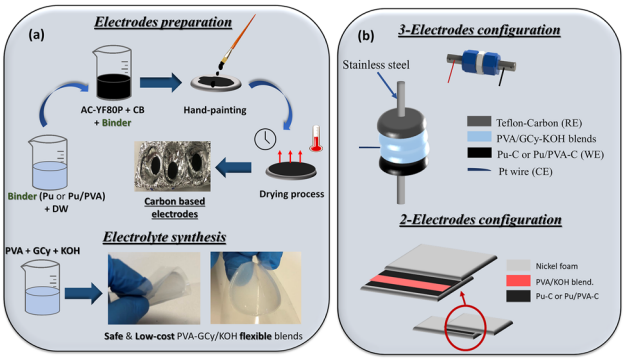

Fig. 1 (a) Carbon based electrodes preparation and PVA-GCy/KOH electrolyte blends synthesis (b) Electrochemical measurements configurations.

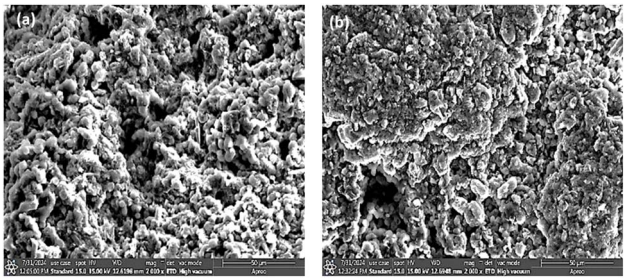

Fig. 2 SEM images, at a scale of 50 μm (a) Pu-C (b) Pu/PVA-C.

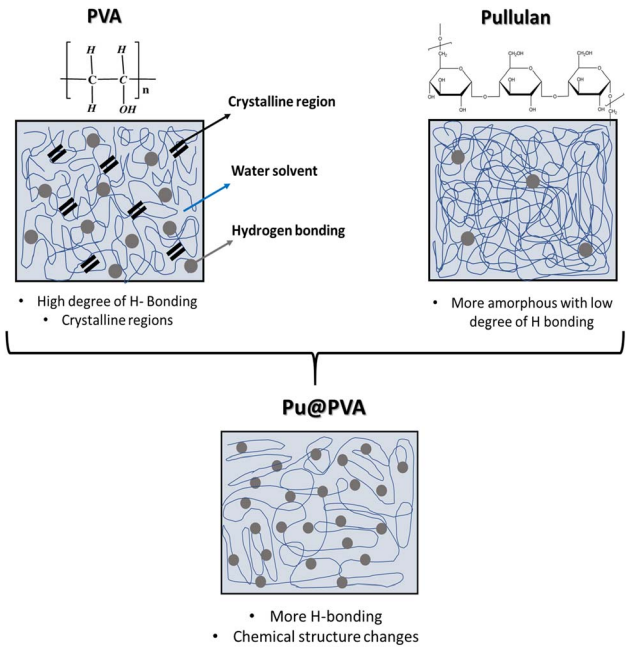

Fig. 3 Schematic illustration of the blending process of Pu with PVA, highlighting the interaction between the polymer chains.

Moreover, the areal capacitances (C_{areal}) as well as the coulombic efficiencies (CE) were evaluated using the following equations.

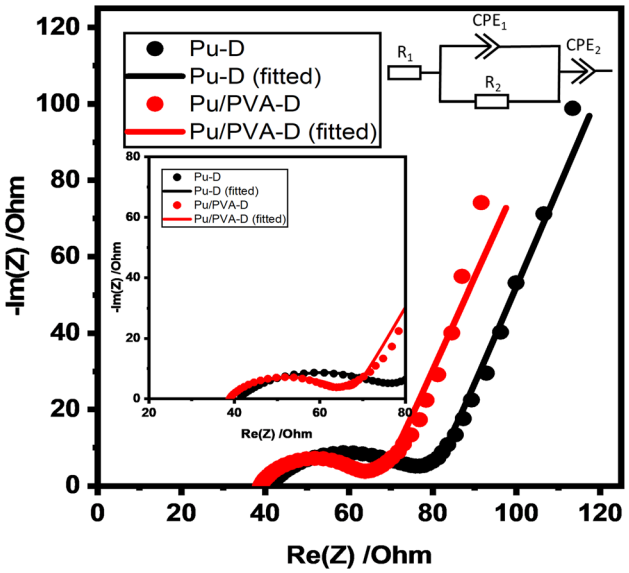

Fig. 4 Nyquist diagrams for Pu-D and Pu/PVA-D from 500 kHz to 100 mHz.

Table 1 Resistances and constant phase elements evaluated by EIS data fitting EIS for Pu-D and Pu/PVA-D supercapacitors

	R_1 (Ω)	R_2 (Ω)	CPE_1 (F s^{n-1})	n_1	CPE_2 (F s^{n-1})	n_2
Pu-D	40.08	41.43	0.013	0.76	0.29 10^{-3}	0.50
Pu/PVA-D	37.92	30.63	0.018	0.75	0.25 10^{-3}	0.55

$$C_{areal} = \frac{\Delta Q\ (\text{Coulomb})}{\Delta V\ (\text{Volts})\ A(\text{cm}^2)} \quad (1)$$

$$\text{CE}(\%) = \frac{Q_{\text{Discharge}}}{Q_{\text{Charge}}} \times 100 \quad (2)$$

where ΔQ is the change in released charge in coulombs, ΔV is the voltage window, A is the electrodes area (cm^2). Q_{Charge} and $Q_{Discharge}$ are the stored and released charges respectively. The device specific capacitances were calculated by dividing the capacitance by the total mass of both electrodes.

3 Results and discussion

3.1 Morphological and structural analyses

Fig. 2 depicts the SEM images of the prepared Pu-C and Pu/PVA-C, at scales of 50 μm. Fig. 2(a) shows that Pu-C reveals amorphous surface with varied shapes and irregular distribution. Conversely, Pu/PVA-C displays a more uniform layer, with the carbon surface showing regular shapes in a more refined and developed manner (Fig. 2(b)). Moreover, both samples show cross linked networks with voids and channels at different sizes and shapes. This further confirms the porosity nature and the highly porous structures with interconnected pores which is in accordance with I.A. Plugariu *et al.* work,[30] in which Pu/PVA hydrogels with different ratios were morphologically and

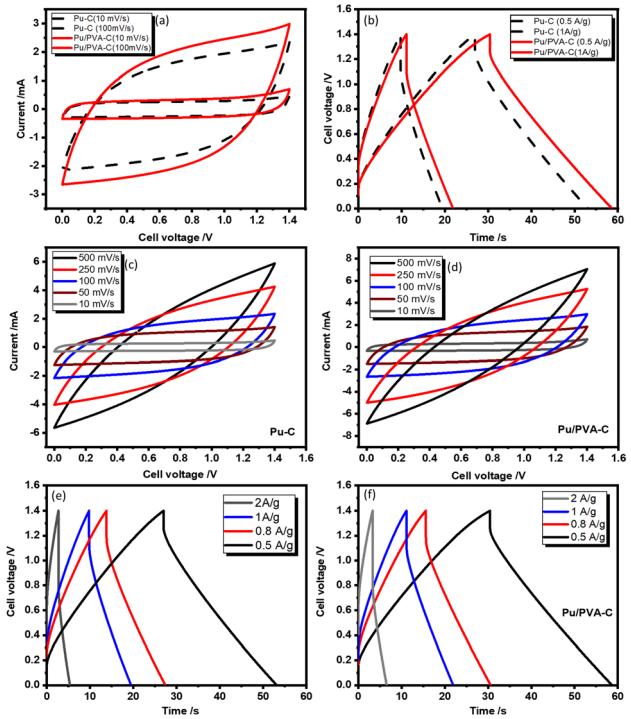

Fig. 5 (a) Cyclic voltammograms at 10 and 100 mV s^{-1} and (b) GCPL profiles at 0.5 and 1 A g^{-1}, for Pu-C and Pu/PVA-C based supercapacitors. (c) and (d) CV at different scan rates and (e) and (f) GCPL with cell cut-off voltage 0–1.4 V, for both devices.

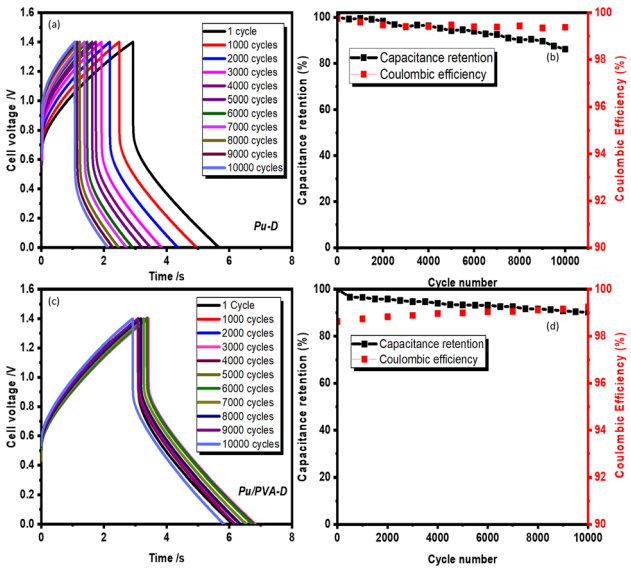

Fig. 6 GCD profiles at all cycles for (a) Pu-D and (c) Pu/PVA-D. Trends of the capacitance retention and CE during 10 000 cycles at 1 A g^{-1}, with cell voltages from 0 to 1.4 V, for (b) Pu-D and (d) Pu/PVA-D respectively.

physically investigated. Moreover, the PVA incorporation effect can be recognized from the blending effects, which is due to the PVA hydroxyl groups (–OH) interactions with Pu. The hydroxyl groups in PVA can form hydrogen bonds with the hydroxyl

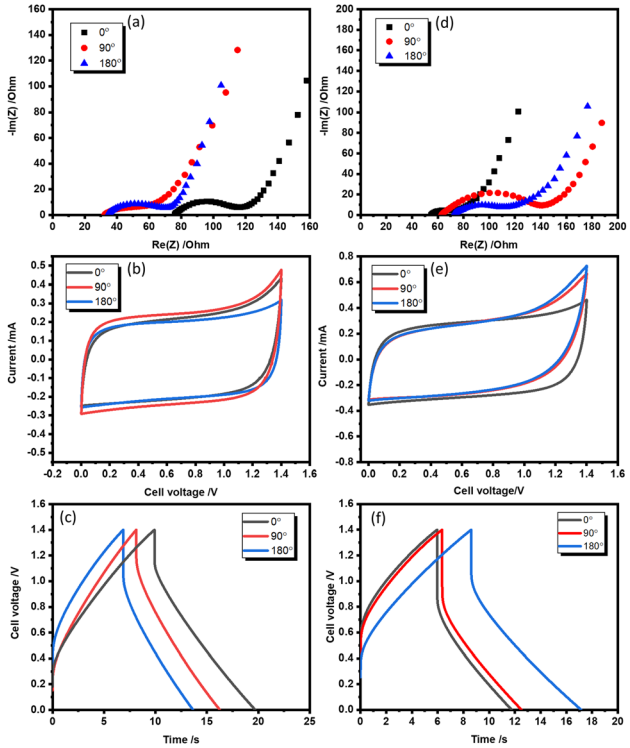

Fig. 7 (a) Nyquist plots (b) cyclic voltammograms at 10 mV s^{-1} and (c) GCPL profiles at 1 A g^{-1} for Pu-D at different bending angles, (d) Nyquist plots (e) cyclic voltammograms at 10 mV s^{-1} and (f) GCPL profiles at 1 A g^{-1} for Pu/PVA-D at different bending angles.

Table 2 Areal and specific capacitances for Pu/PVA-D at 10 mV s^{-1} under different bending angles

Bending angle	Areal capacitance (mF cm^{-2})	Specific capacitance (F g^{-1})
0°	141	35
90°	168	42
180°	174	44

Table 3 Ohmic drop (ΔV), discharge time, ESR, energy and power densities and CE for Pu/PVA-D supercapacitors at 1 A g^{-1} for different bending angles (0°, 90°, 180°)

	ΔV(v)	Δt (s)	ESR (Ω)	C (mF cm^{-2})	P (mW cm^{-2})	E (μWh cm^{-2})	CE (%)
0°	0.42	5.80	91.30	59.80	10.20	16.30	99.00
90°	0.46	6.17	100.00	61.40	9.80	16.70	97.30
180°	0.29	8.55	63.04	74.50	8.80	20.30	96.90

groups in Pu, leading to blending and some degree of interaction at the molecular level. This has been already reported in M.R. Karim *et al.*[24] as well as Plugariu *et al.*[30] works. These findings are further discussed in the SI.

Additionally, compared to Pu-C (Fig. 2(a)), the Pu/PVA-C composite (Fig. 2(b)) exhibits visibly smaller particle features

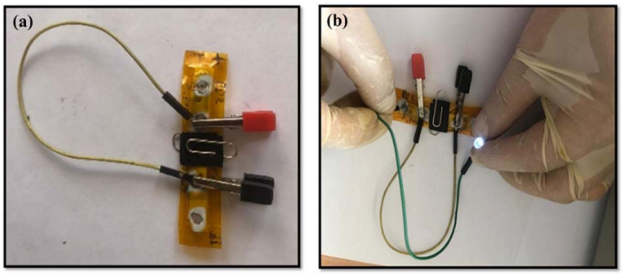

Fig. 8 (a) Series connection of two fabricated Pu/PVA-Carbon supercapacitors (b) 3 V LED powered after charging for 5 minutes to 3 V.

and a more compact and homogeneous surface texture, suggesting a finer dispersion of the active phase within the PVA matrix. The presence of PVA likely limits particle agglomeration during composite formation, leading to reduced particle dimensions and improved distribution. Indeed, Pu is known for its highly amorphous nature,[31] as well as its low degree of hydrogen bonding in its crystal form.[32] This is primarily due to its irregular glycosidic linkages, which prevent ordered packing, while PVA's strong hydrogen bonding allows for some degree of crystallinity (Fig. 3).

Chemically speaking, when PVA is chemically added to Pu, both polymers can form a cross-linked network and interact mainly through hydrogen bonding between the hydroxyl groups of Pu and PVA. This results in a uniform polymer mixture or film. These structural changes lead to enhanced tensile strength and flexibility. The water solubility may be also reduced due to the cross-linking effects, making the blends suitable for humid or aqueous conditions, which, in turn, mitigates the degradation of pure Pu-based films in aqueous electrolytes. Moreover, as depicted in Fig. S1, the Ni Foam spectra demonstrates a characteristic peak at 1586 cm^{-1} wavelength, which is a possible sign of carbonyl groups (C═O Stretching), possibly from adsorbed atmospheric carbon dioxide or contaminants.[33] Vibrations with significant low intensities at the range of 1400–500 cm^{-1} may be attributed to adsorbed organic contaminants and/or residues adsorbed on the foam. Moreover, the Pu-Carbon film exhibits peaks at 790 cm^{-1}, 880 cm^{-1} and 940 cm^{-1} which corresponds to α-(1,4) glucosidic bonds, α-glucopiranosid units and α-(1,6) glucosidic bonds presence. The vibrations at the wavelength range of 1035–1259 cm^{-1} are associated to C–O stretching. Furthermore, CH/CH_2 deformation vibrations can be seen clearly between 1300 and 1506 cm^{-1} wavenumbers. The bands in the range of 2850–3000 cm^{-1} are attributed to the stretching vibrations of CH and CH_2 groups. An exceptionally intense and broad hydroxyl band is observed in the range of 3000–3600 cm^{-1}. These findings are in accordance with several studies such as Md. Shahidul Islam *et al.*,[27] in which the effect of Pu/poly(vinyl alcohol) composites on montmorillonite mineral properties was investigated through several characterization techniques (FTIR,XRD,TEM,TGA). The same trends were also shared by S. Tabasum *et al.* in a comprehensive overview of Pu and its composites, and their applications in food industry, water treatment and pharmaceutical industry.[22] The Pu@PVA-Carbon blends depict almost the same structural behaviour as the bare Pu-based film with slight differences in terms of new peak appearance and intensities variations as discussed in ref. 22–24. By adding PVA, appearance of new peaks at the 1400 cm^{-1} and 1248 cm^{-1} can be recognized. Slight shifts in terms of peak positions may be seen, which are attributed to hydrogen bonding between hydroxyl groups in Pu and those in PVA polymer.

3.2 Three electrodes setup measurements

Fig. S2 compares the Nyquist plots recorded for both electrodes. The low frequency behaviour (1 Hz to 100 mHz) is almost similar: a nearly vertical line is observed for each plot which is a sign of the good capacitive response for both electrodes.[34,35] At the highest frequencies (500 kHz to 1 kHz) the Nyquist plots of both samples show two semicircles, that are typically attributed to the electrode grain boundary resistance and ionic percolation inside the porous electrodes. The intercept of the semi-circle

Table 4 Comparison of areal capacitance, maximum cell voltage, energy and power performances and capacitance retention for the Pu/PVA-D with some reported flexible PVA based solid-state supercapacitors

Structure	C (mF cm^{-2})	ΔV (V)	E (μWh cm^{-2})	P (mW cm^{-2})	Capacitance retention (%)	Ref.
PANI NTs//PVA-H_2SO_4//PANI NTs	237.5	0.6	24.31	2.74	95.2% after 2000 cycles	46
AC//PVA/SA/MXene-NaCl//AC	130.8	—	18.7	0.5	88.9% after 5000 cycles	47
Ti/$K_2Ti_4O_9$@Ni$(OH)_2$//PVA-KOH//Ti/$K_2Ti_4O_9$@Ni$(OH)_2$	5.8	0.8	720	0.16	92.7% after 10 000 cycles	48
LIG//PVA-H_2SO_4//LIG	9.11	1	—	—	98% after 8000 cycles	49
PEDOT-GO/U-C//PVA-H_3PO_4//PEDOT-GO/U-C	30	1	2.2	0.2	89% after 10 000 cycles	50
PANI-ZIF67-CC//PVA-H_2SO_4//PANI-ZIF67-CC	35	1	44	0.245	80% after 2000 cycles	51
CeON/Ni//iPVA-KOH//CeON/Ni	31.82	1.4	—	—	81.2% after 10 000 cycles	52
AC//PVA-PI//AC	130	1	16.7	0.41	95.3% after 10 000 cycles	53
Fe-Tp//PVA-H_2SO_4//Fe-Tp	106.25	1.2	5.31	—	80.0% after 36 000 cycles	54
LIG-CB-Pub//PVA-H2SO4//LIG-CB-Pub	54.4	3	68.1	0.3	95.8% after 6000 cycles	55
Zn–MnO_2@CC//PVA-Na_2SO_4//Zn–MnO_2@CC	81.4	2.25	196	2.38	83% after 4000 cycles	56
AgNPs@CM//KOH(1 M)//PAC	60.4	1.5	18.3	10.237	78.1% after 2000 cycles	57
AC//PVA/GCy-KOH//AC	**92**	**1.4**	**25.0**	**3.2**	**90% after 10 000 cycles**	**This work**

with the real axis at the highest frequency corresponds to the series resistance (R_S) which includes electrode/current collectors and bulk electrolyte resistances. As it is shown, an R_S (2.96 Ω) was obtained for the Pu/PVA-C electrode which was lower than that of the Pu-C based one (42.66 Ω). This huge factor difference (14 times) indicates that the Pu and PVA mixture may contribute strongly to the electrode performance enhancement by enabling higher electrical conductivity and lower internal resistance of the cell. The beneficial effect of the use of Pu/PVA blend can be related to the fine and uniform electrode particle distribution observed by SEM (Fig. 2), which improves contact between conductive components, creating additional percolation pathways for electrons, and increases carbon electrode/electrolyte contact interface. At the mid frequency regions, a non-vertical line (broad knee) is observed for both electrodes, translating the ion transport limitation in the porous structures. This can be attributed to the non-uniform pathways for ion transport from the bulk electrolyte to the surface pores. Furthermore, the intersection of this line with the Re(Z) resulted in a smallest angle for the Pu/PVA-C compared to the Pu-C sample, revealing shorter pathways for ions towards the pores. At the low frequency region, both electrodes exhibited nearly vertical lines revealing the capacitive behaviour dominance of the studied materials.[36,37] More importantly, this low-frequency characteristic increases sharply for the Pu/PVA-C compared to the Pu-C one, which may be a sign of a faster storage and release of electrical charge for the Pu/PVA-C electrode. In Fig. S3, all CV curves shows similar quasi-rectangular shapes within the studied potential window (from −1 to 1 V), with no redox peaks, demonstrating that the capacitive behaviour is driving the electrode response, which is in accordance with the EIS observations.[33] Moreover, higher voltammograms areas were obtained for the Pu/PVA-Carbon electrode which is a sign of higher expected areal capacitances and thus better energy densities within a same applied potential. The maximum achieved areal capacitance was 350 mF cm^{-2} with a coulombic efficiency (CE) of 92.45% from −1 to 0 V for the Pu/PVA-Carbon electrode.

Fig. S4 illustrate the CE of both electrodes in function of the applied potential. The CE of the Pu-C electrode was slightly higher than 99% for $\Delta V = 1.4$ V (99.16% from 0 to 0.5 V and 99.36% from 0 to −0.9 V respectively). For the same potential window, Pu/PVA-C electrode exhibited slightly lower CE values (>95%) which indicates that both electrodes present quite promising properties such as the long lifespan and minimal capacitance losses during cycling.

3.3 Solid state supercapacitor analyses

This section offers insights into the electrochemical performance of Pu-D and Pu/PVA-D symmetric solid-state cells. All fabricated supercapacitors were designed in two electrodes (rectangular shapes) symmetrical configurations within the PGK film sandwiched between the carbon-based electrodes. The active surface area of both electrodes was 0.5 cm^2 with a mass loading (excluding the Nickel foam mass) of 2 mg (Pu-C) and 2.3 mg (Pu/PVA-C) respectively. The electrochemical behaviour of both devices was studied *via* EIS within the range of 100 kHz to 100 mHz and a 10 mV AC perturbation. CV curves were recorded under a cell voltage window of 1.4 V from 10 mV s^{-1} to 500 mV s^{-1} scan rates. GCPL measurements were evaluated from 0 to 1.4 V at different specific current densities 0.5, 0.8, 1 and 2 A g^{-1}.

3.3.1 EIS study. Fig. 4 reports the Nyquist plots recorded within the frequency range of 500 kHz to 100 mHz under 10 mV AC perturbation. Clearly, a similar electrochemical behaviour was observed for both devices. The plots were numerically modeled through the electrical equivalent circuit as illustrated in the inset. All electrochemical/electrical parameters were obtained from Zfit option (EC-Lab V2.17 Software) and are illustrated in Table 1.

CPE_1 and CPE_2 are two constant phase elements which models the non-ideal capacitive behaviour of the system. R_1 is related to the electronic contact resistance, and electrolyte ionic resistance. R_2 refers to percolation resistances (electronic resistance and ions resistance within the pores). The detailed description of the circuital elements is detailed in the SI file. Both devices feature almost similar R_1, which is expected since all samples were assembled and characterized under the same experimental conditions. However, R_2 for Pu/PVA-D is 1.5 times lower than that of Pu-D, revealing improved contact and electrode/electrolyte interface. Lower R_2 indicates faster and more efficient ion adsorption/desorption at the electrode/electrolyte interface, which is beneficial for achieving high energy and power performances.The beneficial effect of the use of Pu/PVA blend can be related to the fine and uniform electrode particle distribution observed by SEM (Fig. 2), which improves contact between conductive components, creating additional percolation pathways for electrons, and increases carbon electrode/electrolyte contact interface.

At the low frequency region, the observed nearly vertical lines for both devices revealed the capacitive behaviour dominance for both structures.[32,34] Moreover, the same performances were perceived as the one seen in the 3-electrodes EIS measurements. Briefly, shorter low-frequency characteristic as well as smallest angle at the intersection of the low frequency line with Re(Z) were observed for the Pu/PVA-C based supercapacitor compared to the Pu-C based one. These findings indicate faster capacitive process for Pu/PVA-D.

Indeed, real-world circuits can be complex with numerous components and interactions. As commonly known, equivalent circuits provide a simplified representation that captures the essential behaviour of the circuit without unnecessary detail. This abstraction makes analysis and design more manageable and understandable. In this context, several other electrical models have been proposed for Nyquist plots modelling when carbon-based supercapacitors are involved.

Table S1 lists some of the possible adopted electrical circuits for describing supercapacitors electrodes/electrolytes interfaces in different electrolytes when carbon materials are employed. In fact, authors typically focus on describing the physico-chemical phenomena occurring at the electrode/electrolyte interfaces through electrical parameters investigations. For instance, the incorporation of the Warburg Impedance element 'Z_W' within

the equivalent circuit represents the diagonal line with a slope of 45° in the low-frequency region of the Nyquist plot. Moreover, electric capacitors are employed to describe the electrodes pure capacitive behaviour which is mostly represented by a vertical line at the low frequency region, starting from the origin of the Nyquist diagram and extending upwards. However, real capacitors often exhibit deviations from this ideal behaviour due to factors such as non-uniform charge distribution, surface roughness, and other imperfections. In such cases, the CPE is used to model systems where the capacitive behaviour deviates from ideality.

3.3.2 Cyclic voltammetry and GCD measurements. The symmetric EDCs were further investigated through the cyclic voltammetry technique and GCPL measurements under different scan rates (from 10 to 500 mV s^{-1}), and current densities (from 0.5 to 2 A g^{-1}), keeping the same 0–1.4 V cell voltage cut off. The voltammograms and GCPL curves for both Pu-C and Pu/PVA-C based devices are reported in Fig. 5. According to the obtained voltammograms, the Pu/PVA-C supercapacitors demonstrate slightly higher currents with larger enclosed area, revealing higher capacitive behaviour. The GCD profiles share almost the same trends with the presence of voltage drops, which are mainly attributed to the PVA-based electrolyte resistance.[38] Indeed, in polymer film electrolytes, ion transport occurs through segmental motion of polymer chains and hopping mechanisms, which are inherently slower than ion diffusion in liquid electrolytes. In addition, the ESR which comprises the intrinsic resistance of the electrode materials, the ionic resistance of the polymer electrolyte, and the interfacial contact resistance at the electrode/electrolyte interfaces, plays a crucial role in governing the magnitude of the IR drop. At low current densities, these resistive contributions are less dominant, resulting in a relatively small voltage drop, whereas at high-rate operation, their combined effect becomes more significant. Furthermore, in solid-state configurations, imperfect interfacial contact and restricted electrolyte penetration into the porous electrode structure can further exacerbate the IR drop under high-current conditions.[38] It is worth noting that current densities of 2 A g^{-1} correspond to 8 mA cm^{-2}, which is relatively extremely high compared to many reported works refs (1.6 mA cm^{-2}),[39], (2 mA cm^{-2}),[40], (1 mA m^{-2})[41] and (7 mA cm^{-2}).[42]

According to Fig. 5(c) and (d), the voltammograms for both devices exhibited the same quasi-rectangular and symmetrical profiles. Indeed, the shape transition from the nearly rectangular (low scan rates) to the distorted profiles (high scan rates) translates the nonideal cycling behaviour during measurements. It was also reported by D. Bookpandee *et al.*,[43] that the blunt and slanted shapes of the obtained voltammograms are mainly due to imperfections and uneven ions redistribution when LiCl/PVA gels are employed as ionic mediums. These results are in accordance with the GCPL curves illustrated in Fig. 5(e) (for Pu-D) and 5(f) (for Pu/PVA-D). Indeed, symmetrical and linear triangular-like shapes are observed for almost all studied current densities, revealing the excellent reversibility and the good EDLC behaviour.[44,45] The maximum calculated areal capacitances were 176 mF cm^{-2} (44 F g^{-1}) for the Pu/PVA-D and 126 mF cm^{-2} (32 F g^{-1}) for the Pu-D, at 10 mV s^{-1}. The areal capacitances at 50 and 100 mV s^{-1} were, 121 mF cm^{-2} (30 F g^{-1}) and 103 mF cm^{-2} (26 F g^{-1}) for the Pu/PVA-D. Pu-D exhibited only 95 mF cm^{-2} (24 F g^{-1}) and 81 mF cm^{-2} (20 F g^{-1}) at the same experimental conditions.

The supercapacitor KPIs, including the voltage drop (ΔV), discharge time (Δt), power (P) and energy (E) densities and the coulombic efficiency (CE) were calculated at 0.5 A g^{-1} for both devices and are reported in table S2. The highest energy densities were obtained for the Pu/PVA-D (25 μWh cm^{-2}) which is mainly related to the higher areal capacitance (92 mF cm^{-2}) found for this latter. The coulombic efficiencies for both devices were above 90% implying the excellent charge/discharge process at the electrode/electrolyte interfaces. In addition, slightly higher power densities were reached for this latter compared to the Pu-D based device, which is related to the better electron pathway created by the Pu and PVA groups interactions which is in accordance with the lower electrode percolation obtained from the EIS measurements. Both devices exhibited a good CE (>95%) revealing the good interfacial stability between the carbon electrode and the polymer films.

The capacitance retention rate was evaluated for both supercapacitors after 10 000 charging/discharging cycles at room temperature through GCPL measurements at 1 A g^{-1} from 0 to 1.4 V, at room temperature. The GCD profiles at different cycles are illustrated in Fig. 6(a) (Pu-D) and 6(c) (Pu/PVA-D). Fig. 6(b) and (d) illustrates the trend of the capacitance retention as well as the coulombic efficiency (CE) evolution during measurements. Both devices showed excellent stability features (>90%) after 10 000 cycles with a slight superiority for Pu/PVA-D based device. The capacitance retention for Pu-D and Pu/PVA-D maintained 86.1% and 90.3% after 10 000 cycles with a CE of 99.4% and 99.3% respectively. These findings prove that alongside the ecological aspect, the excellent stability against the dissolution in water and the biocompatibility, Pu/PVA composites may be considered as novel and attractive binders toward high lifespan and long-life service carbon-based solid-state supercapacitors.

3.3.3 Flexibility tests. The mechanical strength of the fabricated devices was electrochemically evaluated at different bending angles (0°, 90° and 180°) as depicted in Fig. S5. Fig. 7 illustrates all the electrochemical measurements for both devices at the normal position and/or bended, under room temperature conditions.

Fig. 7(a) and (d) illustrate the Nyquist diagrams for the Pu-D and Pu/PVA-D respectively at different bending angles. As shown, The ESRs and the low frequency characteristics differ when both devices were folded but a clear trend with the bending angle cannot be claimed. However, the voltammograms shown in Fig. 6(b) and (e) do not show significative differences under bending for both devices, revealing the good capacitive behaviour discussed in the previous sections. The areal capacitances for both devices were calculated at 10 mV s^{-1} and are illustrated in Table 2. While for Pu-D, capacitance decreases when increasing the bending angle, for Pu/PVA-D the opposite trend is observed. At 0° angle, Pu-D demonstrated an aerial capacitance of 122 mF cm^{-2} (30 F g^{-1}), while Pu/PVA-D

exhibited a capacitance of 141 mF cm^{-2}(35 F g^{-1}). Unlike Pu-D, Pu/PVA-D capacitance increases to 168 (42 F g^{-1}) and then to 174 mF cm^{-2} (44 F g^{-1})at 90° and 180° respectively. The Pu-D areal capacitance decreased to 114 mF cm^{-2} (29 F g^{-1}) and 95 mF cm^{-2} (24 F g^{-1}) at the same bending angles confirming the reciprocal trend. These results are probably due to the better interfacial contact and an enhanced exposure rate of the active material surface to the electrolyte film surface which is probably a result of the generated mechanical pressure when the Pu/PVA-D was folded.

The different trend of capacitance under folding of Pu/PVA and PVA-based devices can be explained referring to the different properties of the corresponding electrode binders. PVA enhances mechanical flexibility and maintains good contact between electrode components under bending, which can improve conductive pathways and slightly increase capacitance. In contrast, pure Pu-based devices are more brittle, a known limitation of pullulan, so bending can easily cause micro-cracks or partial separation of components, with negative effect on electron and ion transport and leading to a decrease in capacitance.

Furthermore, energy and power densities, as well as the CE were calculated from GCPL measurements at a current density of 1 A g^{-1} from 0 to 1.4 V and the corresponding values are summarized in Table 3. The Pu-D supercapacitor shows no substantial changes in its energy performances, with only a slight decrease in capacitance as the bending angle increases. For instance, Pu-D demonstrated a capacitance of 55 mF cm^{-2} (14 F g^{-1}) at 0°, which decreased to only 51 mF cm^{-2} (13 F g^{-1}) at 180°. Instead, according to Table 3, the capacitance for Pu/PVA-D increases from 60 mF cm^{-2} (15 F g^{-1}) (0°) to 75 mF cm^{-2} (19 F g^{-1}) (180°). Also, ESR decreases when the device was folded. Accordingly, enhancements in terms of energy and power densities were noticed when the Pu/PVA-D was bended. A maximum energy density of 20 μWh cm^{-2} and power density of 9 mW cm^{-2} were recorded for the 90° and 180° angles with a CE higher than 96%.

These findings support the fact that Pu/PVA blending composites may be promising as ecological binders towards the development of solid-state supercapacitors with excellent mechanical strength, opening great potential application in smart textile technology and offering the chance of large-scale production for the electronics market.

The proficiency and potential applications of our fabricated devices were evaluated through supplying a 3 V LED diode using 2-connected supercapacitors in series as shown in Fig. 8.

The electrochemical performance of the AC//PVA/GCy-KOH//AC symmetric device developed in this work compares favourably with recently reported flexible and solid-state supercapacitors (Table 4).

Although some systems, exhibit higher areal capacitances (237.5 mF cm^{-2})[46] (130.8 mF cm^{-2}),[47] they typically operate within a narrower voltage window (≤0.6 V) and suffer from limited long-term stability due to the intrinsic degradation of conducting polymers and involvement of MXene materials.

In contrast, the present device delivers a balanced areal capacitance of 91.6 mF cm^{-2} while operating at an extended voltage window of 1.4 V, resulting in a competitive areal energy density of 25.0 μWh cm^{-2} and a high-power density of 3.2 mW cm^{-2}. These values are comparable to or exceed those of many reported carbon-based and hybrid systems,[48–53] including PEDOT-GO-based,[50] AC//PVA-PI,[53] and MXene-containing devices, which often trade power capability for energy density.

Other systems demonstrated excellent KPIs; however, these performances were often achieved through the incorporation of metal oxides and the use of complex synthesis routes and advanced instrumentation.[54–57] Furthermore, the device retains ~90% of its initial capacitance after 10 000 charge–discharge cycles, demonstrating excellent electrochemical stability that surpasses or rivals most polymer- and metal-oxide-based counterparts. This combination of moderate-to-high capacitance, wide operating voltage, and robust cycling stability highlights the effectiveness of the GCy-modified PVA-KOH electrolyte and confirms the suitability of the proposed architecture for practical solid-state energy-storage applications.

4 Conclusions

Flexible electronics including wearable technologies require light and safe power sources with high-rate performances and long cycle life. Overall, the highlights of this work include the following points: (i) the use of safe and ecological PVA based films as potential electrolytes instead of complex blends and/or acidic mediums which are generally harmful, unsafe and limits the devices life cycle (ii) no critical conditions were needed during the electrode fabrication since no heavy metals, toxic solvents or functionalized nanomaterials were involved revealing the simplicity and the eco-friendly aspects of the manufacturing technique.

Indeed, in this work, through a simple and low-cost hand painting manufacturing process, we demonstrated the use of Pu/PVA composites as a green binder, for the first time for supercapacitors carbon-based electrodes development. Moreover, PVA-KOH blends plasticized with GCy have been first employed as hydrogel films for supercapacitors fabrication. Pu/PVA based supercapacitor showed slightly superior energetic performance compared to the neat Pu based one. Along with the excellent stability and reversibility, no performances degradation was found for this latter under different bending angles revealing the excellent mechanical properties. In summary, Pu/PVA composites may be considered as one of the best candidates for carbon-based electrodes development for supercapacitors and batteries industries. Besides, we believe that the fabricated devices present great potential for use in next-generation flexible and portable energy-storage devices.

Author contributions

Elyes Bel Hadj Jrad: conceptualization, methodology, formal analysis, investigation, visualization, writing – original draft. Francesca Soavi: conceptualization, supervision, investigation, resources, validation, formal analysis, writing – review & editing. Chérif Dridi: conceptualization, supervision, project

administration, resources, validation, writing – review & editing, funding acquisition.

Conflicts of interest

The authors declare that they have no conflicts to declare.

Data availability

Data for this article are available at https://amsacta.unibo.it/id/eprint/8800. Supplementary information (SI): Fig. S1 represents the FTIR spectrum of pure PVA, pullulan-carbon and pullulan/PVA-carbon composites respectively. Fig. S2 shows the Nyquist plot of both pullulan-carbon and pullulan/PVA-carbon in a three electrodes system from 100 KHz to 100 mHz. Fig. S3 demonstrates the working potential window for both pullulan/carbon, and pullulan/pVA-carbon in a three electrodes system setup from −1 to 1 V *vs.* ref. Fig. S4 shows the coulombic efficiency variations of the studied materials. Table S1 demonstrates some adopted electrical equivalent circuits that model the electrochemical behavior of supercapacitors including the one adopted for this study, with related explanations on the electrical components of our adopted electrical circuit and their definitions. Table S2 shows the KPIs of the developed supercapacitors extracted from galvanostatic charge/discharge measurements at 0.5 A g^{-1}. Fig. S5 illustrates real images of the developed supercapacitors under different bending angles. See DOI: https://doi.org/10.1039/d5ta07754k.

Acknowledgements

The authors would like to thank the Tunisian MHESR for supporting this work and the University of Sousse for the "Bourse d'Alternance" fellowship awarded to Mr Elyes Bel Hadj Jrad. F. S acknowledges MOST – Sustainable Mobility Center project, funded by the European Union Next-GenerationEU (PIANO NAZIONALE DI RIPRESA E RESILIENZA (PNRR) e MISSIONE 4 COMPONENTE 2, INVESTIMENTO 1.4 e D.D. 1033 17/06/2022, CN00000023). This manuscript reflects only the authors' views and opinions, neither the European Union nor the European Commission can be considered responsible for them.

Notes and references

1 MarketsandMarkets Team, Supercapacitor market by type (Double layer capacitors, Pseudocapacitors, Hybrid capacitors : Attractive opportunities in supercapacitor market, 2023.
2 International Energy Agency, Global and regional percentage changes in electricity demand, 2023.
3 A. Kalair, N. Abas, M. S. Saleem, A. R. Kalair and N. Khan, *Energy Storage*, 2021, **3**, e135.
4 P. E. Lokhdan and U. S. Chavan, Inorganic Electrolytes in Supercapacitors, In *Materials Research Foundations*, Materials Research Forum LLC, 2019, vol. 61.
5 A. Mert and Z. Xiangyang, *Int. J. Energy Res.*, 2022, 10389–10452.
6 A. Kumar, H. K. Rathore, D. Sarkar and A. Shukla, *Electrochem. Sci. Adv.*, 2022, **2**, e2100187.
7 P. H. Patil, V. V. Kulkarni and S. A. Jadhav, *J. Compos. Sci.*, 2022, **6**, 363.
8 T. Divya, R. Sarankumar, K. S. Balamurugan, P. Sakthivel and A. Sivakami, *J. Nanoparticle Res.*, 2025, **27**, 55.
9 A. Huang, Y. He, Y. Zhou, Y. Zhou, Y. Yang, J. Zhang, L. Luo, Q. Mao, D. Hou and J. Yang, *J. Mater. Sci.*, 2019, **54**, 949–973.
10 D. Bergna, T. Varila, H. Romar and U. Lassi, *C*, 2018, **4**, 41.
11 Z. Xu, D. Zhang, X. Liu, Y. Yang, X. Wang and Q. Xue, *Nano Energy*, 2022, **94**, 106881.
12 H. Deng, Z. Wang, M. Kim, Y. Yamauchi, S. J. Eichhorn, M.-M. Titirici and L. Deng, *Nano Energy*, 2023, **117**, 108914.
13 E. Bel Hadj Jrad, A. Elmouwahidi, E. Bailón García, F. Carrasco Marín and C. Dridi, *J. Power Sources*, 2025, **654**, 237871.
14 Y. Yang, Y. Liu, B. Deng, Y. Li, B. Yin and M. Yang, *Electrochim. Acta*, 2023, **440**, 141751.
15 D. Kasprzak and M. Galiński, *J. Power Sources*, 2023, **553**, 232300.
16 A. Brilloni, F. Poli, G. E. Spina, C. Samorì, E. Guidi, C. Gualandi, M. Maisuradze, M. Giorgetti and F. Soavi, *Electrochim. Acta*, 2022, **418**, 140376.
17 F. Poli, D. Momodu, G. E. Spina, A. Terella, B. K. Mutuma, M. L. Focarete, N. Manyala and F. Soavi, *Electrochim. Acta*, 2020, **338**, 135872.
18 E. Petri, M. Arnaiz, C. Gualandi, F. Soavi and J. Ajuria, *J. Power Sources*, 2025, **657**, 238177.
19 G. E. Spina, F. Poli, A. Brilloni, D. Marchese and F. Soavi, *Energies*, 2020, **13**, 3115.
20 A. Brilloni, F. Marchesini, F. Poli, E. Petri and F. Soavi, *Energies*, 2022, **15**, 2608.
21 S. Alipoori, S. Mazinani, S. H. Aboutalebi and F. Sharif, *J. Energy Storage*, 2020, **27**, 101072.
22 S. Tabasum, A. Noreen, M. F. Maqsood, H. Umar, N. Akram, Z.-H. Nazli, S. A. S. Chatha and K. M. Zia, *Int. J. Biol. Macromol.*, 2018, **120**, 603–632.
23 E. Bel Hadj Jrad, F. Soavi and C. Dridi, *J. Energy Storage*, 2024, **88**, 111471.
24 M. R. Karim and Md. S. Islam, *J. Nanomater.*, 2011, **2011**, 1–7.
25 I. Samoila, S. Dinescu, G. G. Pircalabioru, L. Marutescu, G. Fundueanu, M. Aflori and M. Constantin, *Materials*, 2019, **12**, 3220.
26 N. Teramoto, M. Saitoh, J. Kuroiwa, M. Shibata and R. Yosomiya, *J. Appl. Polym. Sci.*, 2001, **82**, 2273–2280.
27 Md. S. Islam, J. H. Yeum and A. K. Das, *J. Colloid Interface Sci.*, 2012, **368**, 273–281.
28 Md. S. Islam and J. H. Yeum, *Colloids Surf., A*, 2013, **436**, 279–286.
29 K. Zhang, J. Sun, L. E, C. Ma, S. Luo, Z. Wu, W. Li and S. Liu, *J. Energy Storage*, 2022, **45**, 103457.
30 I.-A. Plugariu, M. Bercea, L. M. Gradinaru, D. Rusu and A. Lupu, *Gels*, 2023, **9**, 580.
31 E. Kristo and C. Biliaderis, *Carbohydr. Polym.*, 2007, **68**, 146–158.

32 R. Y. Lochhead, in *Cosmetic Science and Technology*, Elsevier, 2017, pp. 171–221.
33 S. Sudhasree, A. Shakila Banu, P. Brindha and G. A. Kurian, *Toxicol. Environ. Chem.*, 2014, **96**, 743–754.
34 R. Manikandan, C. J. Raj, M. Rajesh, B. C. Kim, J. Y. Sim and K. H. Yu, *ChemElectroChem*, 2018, **5**, 101–111.
35 E. B. Hadj Jrad, A. Elmouwahidi, E. B. García, F. C. Marín and C. Dridi, *Inorg. Chem. Commun.*, 2026, **186**, 116099.
36 I. Shaheen, K. S. Ahmad, C. Zequine, R. K. Gupta, A. G. Thomas and M. A. Malik, *J. Mater. Sci.*, 2020, **55**, 7743–7759.
37 R. Shah, X. Zhang and S. Talapatra, *Nanotechnology*, 2009, **20**, 395202.
38 M. M. Amaral, R. Venâncio, A. C. Peterlevitz and H. Zanin, *J. Energy Chem.*, 2022, **67**, 697–717.
39 R. Rostami and M. Faraji, *J. Inorg. Organomet. Polym. Mater.*, 2020, **30**, 3438–3447.
40 Y. Xie and J. Wang, *J. Sol-Gel Sci. Technol.*, 2018, **86**, 760–772.
41 Y. Chen, W. Yang, D. Yang, P. Wangyang and X. Li, *J. Mater. Sci. Mater. Electron.*, 2019, **30**, 6350–6357.
42 C. Boucher, O. Rubel and I. Zhitomirsky, *Molecules*, 2023, **28**, 1562.
43 D. Boonpakdee, C. F. Guajardo Yévenes, W. Surareungchai and C. La-o-vorakiat, *J. Mater. Chem. A*, 2018, **6**, 7162–7167.
44 F. Shao, N. Hu, Y. Su, L. Yao, B. Li, C. Zou, G. Li, C. Zhang, H. Li, Z. Yang and Y. Zhang, *Chem. Eng. J.*, 2020, **392**, 123692.
45 Y. Liu, X. Zhai, K. Yang, F. Wang, H. Wei, W. Zhang, F. Ren and H. Pang, *Front. Chem.*, 2019, **7**, 118.
46 H. Li, J. Song, L. Wang, X. Feng, R. Liu, W. Zeng, Z. Huang, Y. Ma and L. Wang, *Nanoscale*, 2017, **9**, 193–200.
47 J. Tian, Z. Sun, C. Shi and Z. Huang, *Int. J. Biol. Macromol.*, 2023, **248**, 125937.
48 W. Zhou, X. Liu, Y. Sang, Z. Zhao, K. Zhou, H. Liu and S. Chen, *ACS Appl. Mater. Interfaces*, 2014, **6**, 4578–4586.
49 Z. Peng, J. Lin, R. Ye, E. L. G. Samuel and J. M. Tour, *ACS Appl. Mater. Interfaces*, 2015, **7**, 3414–3419.
50 D. Fu, H. Li, X.-M. Zhang, G. Han, H. Zhou and Y. Chang, *Mater. Chem. Phys.*, 2016, **179**, 166–173.
51 L. Wang, X. Feng, L. Ren, Q. Piao, J. Zhong, Y. Wang, H. Li, Y. Chen and B. Wang, *J. Am. Chem. Soc.*, 2015, **137**, 4920–4923.
52 U. N. Kumar, S. Ghosh, C. R. Jeevandoss and T. Thomas, *J. Energy Storage*, 2023, **74**, 109563.
53 Q. Zhou, A. Griffin, J. Qian, Z. Qiang, B. Sun, C. Ye and M. Zhu, *Adv. Funct. Mater.*, 2024, **34**, 2405962.
54 A. Khayum Mohammed, A. Pandikassala, P. Pena Sánchez, S. Abdullah Gaber, S. Canossa, M. Kurian, G. Xavier, Y. He, F. Gándara, S. Kurungot and D. Shetty, *Chem. Eng. J.*, 2024, **496**, 153589.
55 S. Baachaoui, W. Mabrouk, O. Ghodbane and N. Raouafi, *J. Energy Storage*, 2024, **75**, 109580.
56 M. M. Momeni and N. Moosavi, *J. Alloys Compd.*, 2024, **1006**, 176257.
57 S. C. Sekhar, G. Nagaraju, B. Ramulu and J. S. Yu, *ACS Appl. Mater. Interfaces*, 2018, **10**, 36976–36987.